

The numerical simulation of sediments ground motion on variation in thickness and wave velocity

Li Yiqiong, Yu Yanxiang

Institute of Geophysics, China Earthquake Administration, Beijing, China

Abstract

The work is proposed by the actual needs of engineering seismology. Sedimentary basins provide several propagation paths for seismic wave, which can lead to the reflected wave from basin margin and the gathered wave in the center of the basin. The seismic wave is strengthened or weakened at different positions of basin. Basin amplification effects are caused by several factors including the thickness of sedimentary basin, basin geometry and basin velocity interface. Numerical simulation is helpful for us to quantitatively analysis the specific reason for the basin effects.

We implement long-period ground motions numerical simulation affected by the basin structure by using previous developed structure-preserving algorithm, symplectic discrete singular convolution differentiator (SDSCD), to simulate propagation of seismology fields; using far-field earthquake input; and adopting perfectly matched layers (MPL) absorbing boundary condition. We quantitatively study the impact of the basin model parameters to ground motions peak value, response spectrum and duration by constructing several basin models to obtain strength level of space-time changes on amplification effects.

It will lay the foundation on making reasonable adjustment for ground motion parameter of sedimentary basin area and on making prior estimation for possible earthquake damage.

Introduction

Ground motion is the product of the complex system including source, seismic wave propagation and site effects in Earth medium. Ground motion study covers theoretical seismology and engineering seismology, which has not only theoretical significance, but also application value. On the one hand, near-field strong motion records contain the

details of source activity; therefore, analyzing near-field strong ground motion records has been available to research focal process. On the other hand, strong ground motion perhaps directly contributes to earthquake disaster. Due to above two reasons, the circles of theoretical seismology and engineering seismology pay great attention to ground motion research, which has become a more active research area and has gotten great development.

In the early years, ground motion simulations have shown significant basin amplification effects including simplified source implementations such as plane waves or line/point sources. Frankel and Vidale (1992) considered two cases: an explosion source and a double force-couple source to simulate propagation of elastic waves through the Santa Clara Valley using finite-difference method. It is well known that sites in sedimentary basins experience large ground motions with longer durations than do sites on rock (e.g., Yomogida and Etgen, 1993; Olsen and Schuster, 1995). These results were confirmed by more detailed simulations including the finite-fault source effects. Olsen and Archuleta (1996) simulated the earthquakes on the Los Angeles fault system. Frankel and Stephenson (2000) computed the ground motion in Seattle region. In these works we find that the simulations focus on the certain basin regions and the relevant realistic earthquakes. Therefore, the realistic ground motion records can be compared with numerical results to verify the simulation methods. However, basin amplification patterns are generally different and are not quantitatively available from one basin to another. The cycle of earthquake engineering is more concerned with the amplification level contributed to large structural damage during moderate to large earthquakes. Moreover, we need estimate hazard level of ground motion for earthquake-resistant design or post-disaster relief. In view of the above-mentioned facts, we expect to make certain of the basic law of basin effects on characteristic models rather than certain realistic basin areas. The seismic response including the generation of surface waves and localized resonances depends strongly on the properties of the basin, such as wave velocities, geometry of the structure. Of course, the location of the source and its patterns also are important facts in the response. In this work, we build the basin models with various dimensionless

frequencies, that is the ratio of the basin width and incident wavelength, to simulate the seismic response by using previous developed symplectic discrete singular convolution differentiator (SDSCD) algorithm. The SDSCD algorithm has shown strong stability due to the structure preserving symplectic scheme and localized spatial differentiator (Ma, 2010; Li, 2011; Li 2012). The numerical results also confirm that the algorithm has the superior performance to solve long-time simulation problems.

As an example, we apply the SDSCD to seismic elastic wave-field modeling in basin characteristic models with P-SV plane wave incidence. From these numerical results, we find that Rayleigh surface wave can be confirmed. The numerical results also show that the basin effects are sensitive to depth and wave velocity of basin. Ground motions are amplified at basin margin and the center of the basin compared with homogeneous layered model.

Theoretical Method

SDSCD Scheme

Generally, the elastic equation for two-dimensional P-SV wave in the time domain can be written as

$$\left\{ \begin{array}{l} \rho \frac{\partial v_x}{\partial t} = \frac{\partial \sigma_{xx}}{\partial x} + \frac{\partial \sigma_{xz}}{\partial z} \\ \rho \frac{\partial v_z}{\partial t} = \frac{\partial \sigma_{zx}}{\partial x} + \frac{\partial \sigma_{zz}}{\partial z} \\ \frac{\partial \sigma_{xx}}{\partial t} = (\lambda + 2\mu) \frac{\partial v_x}{\partial x} + \lambda \frac{\partial v_z}{\partial z} \\ \frac{\partial \sigma_{zz}}{\partial t} = \lambda \frac{\partial v_x}{\partial x} + (\lambda + 2\mu) \frac{\partial v_z}{\partial z} \\ \frac{\partial \sigma_{xz}}{\partial t} = \mu \frac{\partial v_x}{\partial z} + \mu \frac{\partial v_z}{\partial x} \\ \frac{\partial \sigma_{zx}}{\partial t} = \mu \frac{\partial v_x}{\partial z} + \mu \frac{\partial v_z}{\partial x} \end{array} \right. , \quad (1)$$

Where v_x and v_z are respectively the wave filed velocity of x and z axes. σ_{xx} , σ_{zz} , σ_{xz} and σ_{zx} are stress components, ρ is media density, λ and μ are media

elastic parameters.

In the convolutional differentiator method, the spatial derivatives of arbitrary $u(x, z, t)$ can be written as

$$\frac{\partial u(x, z, t)}{\partial x} = \hat{d}_1(x) * u(x, z, t), \quad (2)$$

where $*$ stands for the convolution with respect to x and $\hat{d}_1(x)$ is the convolutional differentiator for the first-order derivative. For seismic modeling in the discrete domain, generally, the solution of the seismic elastic wave in equation (1) can be written as

$$\begin{cases} v_x(m, n, t + \Delta t) = v_x(m, n, t) + \frac{1}{\rho(m, n)} \Delta t [\Delta x L_x(\sigma_{xx}) + \Delta z L_z(\sigma_{xz})] \\ v_z(m, n, t + \Delta t) = v_z(m, n, t) + \frac{1}{\rho(m, n)} \Delta t [\Delta x L_x(\sigma_{zx}) + \Delta z L_z(\sigma_{zz})] \\ \sigma_{xx}(m, n, t + \Delta t) = \sigma_{xx}(m, n, t) + (\lambda + 2\mu) \Delta t \Delta x L_x(v_x) + \lambda \Delta t \Delta z L_z(v_z), \\ \sigma_{zz}(m, n, t + \Delta t) = \sigma_{zz}(m, n, t) + \lambda \Delta t \Delta x L_x(v_x) + (\lambda + 2\mu) \Delta t \Delta z L_z(v_z) \\ \sigma_{xz}(m, n, t + \Delta t) = \sigma_{xz}(m, n, t) + \mu \Delta t \Delta z L_z(v_x) + \mu \Delta t \Delta x L_x(v_z) \\ \sigma_{zx}(m, n, t + \Delta t) = \sigma_{zx}(m, n, t) + \mu \Delta t \Delta z L_z(v_x) + \mu \Delta t \Delta x L_x(v_z) \end{cases} \quad (3)$$

where m and n are indices along the discrete x and z axes; Δx , Δz , and Δt are sampling rates along the x , z , and t axes; L_x , L_z are discrete single convolution differentiator along the x and z axes. Applying the differentiator to arbitrary $u(x, z, t)$, we can obtain

$$L_x(u(m, n, t)) = \sum_{i=-mx}^{mx} \hat{d}_1(i\Delta x) u(m-i, n, t), \quad (4)$$

$$L_z(u(m, n, t)) = \sum_{j=-nz}^{nz} \hat{d}_1(j\Delta z) u(m, n-j, t), \quad (5)$$

where mx and nz are the half differentiator lengths in sampling number along the x and z axes.

Applying an explicit third-order partitioned Runge-Kutt temporal discretization scheme (Iwatsu, 2009) to equation (3), we can obtain

$$\begin{aligned}
V_1 &= V^n + \Delta t c_1 P(U^n), \quad U_1 = U^n + \Delta t d_1 Q(V_1), \\
V_2 &= V_1 + \Delta t c_2 P(U_1), \quad U_2 = U_1 + \Delta t d_2 Q(V_2), \\
V^{n+1} &= V_2 + \Delta t c_3 P(U_2), \quad U^{n+1} = U_2 + \Delta t d_3 Q(V^{n+1}),
\end{aligned} \tag{6}$$

where $V^{n+1} = (v_x(m, n, t + \Delta t), v_z(m, n, t + \Delta t))^T$,

$$U^{n+1} = (\sigma_{xx}(m, n, t + \Delta t), \sigma_{zz}(m, n, t + \Delta t), \sigma_{xz}(m, n, t + \Delta t), \sigma_{zx}(m, n, t + \Delta t))^T,$$

$$P = \begin{pmatrix} \frac{1}{\rho} \Delta x L_x & 0 & \frac{1}{\rho} \Delta z L_z & 0 \\ 0 & \frac{1}{\rho} \Delta z L_z & 0 & \frac{1}{\rho} \Delta x L_x \end{pmatrix},$$

$$Q = \begin{pmatrix} (\lambda + 2\mu) \Delta x L_x & \lambda \Delta z L_z \\ \lambda \Delta x L_x & (\lambda + 2\mu) \Delta z L_z \\ \mu \Delta z L_z & \mu \Delta x L_x \\ \mu \Delta z L_z & \mu \Delta x L_x \end{pmatrix},$$

$$c_1 = \frac{1}{12} \left(\sqrt{\frac{209}{2}} - 7 \right), c_2 = \frac{11}{12}, c_3 = \frac{1}{12} \left(8 - \sqrt{\frac{209}{2}} \right),$$

$$d_1 = \frac{2}{9} \left(1 + \sqrt{\frac{38}{11}} \right), d_2 = \frac{2}{9} \left(1 - \sqrt{\frac{38}{11}} \right), d_3 = \frac{5}{9}.$$

Equation (6) is an explicit third-order symplectic discrete singular convolution differentiator scheme, that is called SDSCD scheme. A common method to measure the efficiency of the algorithm is to discuss the grid point number per shortest wavelength without any grid dispersion. It is verified that pseudo-spectrum algorithm only need two grid points per shortest wavelength (Kosloff, 1982). Our SDSCD scheme also needs only two grid points per shortest wavelength. In actual calculation, we usually set three or four grid points per shortest wavelength.

Plane Wave Incidence

We consider the input wave motion applied on the bottom of the computational area, which is transformed into an equivalent load. We load the equivalent force into

displacement of each bottom point as P-SV wave incidence. Wave incidence is solved by using the approach of Virieux (1984). For plane-wave excitation, the incident displacement can be given by a wavelet or a seismic record. The incident displacement is given by a Ricker wavelet as

$$f(x, z, t) = f(x, z_s, t) = \left[1 - 2(\pi f_p (t - t_0))^2 \right] \exp \left[-(\pi f_p (t - t_0))^2 \right], \quad (7)$$

where, $f(x, z_s, t)$ is just applied at $z = z_s$, z_s is the location of plane-wave incidence, f_p is peak frequency, t_0 is time delay, t_0 ensure that starting time of wavelet do not value negative.

Boundary Condition

Absorbing boundary conditions are used to mitigate undesired reflections from the model's truncation boundaries in time domain modeling. The perfectly matched layer (PML) is generally acknowledged as the available absorbing boundary condition and efficient to absorb both wave and surface waves. Since Berenger (1994) proposed PML for electromagnetic wave equation, PML boundary condition has been widely extended in wave field simulation by a number of researchers. There are several equivalent formulations of PML. Berenger's original formulation is called the split-field PML (SPML), because he artificially split the wave solutions into the sum of two new artificial field components. Another common formulation is the non-splitting PML (NPML). Both the SPML and NPML formulations can be derived by viewing them as the result of a complex coordinate stretching. In this paper, we use the modified NPML formulation by Qin (2009), which is a simple and efficient NPML based on non-convolution technology.

Algorithm Validation

Classic theory of seismology tells us when the plane wave is incident to the surface in homogeneous medium, the surface displacement is constant twice of the incident wave displacement. We validate the theory by designed experiment. Plane wave is vertically incident to the surface from the bottom of homogeneous medium. The excitation is Ricker

wavelet. The displacement records of incident wave and surface receiver are showed in

Fig.1 and Fig.2. We define the ratio of peak value between input and output $\tau = \frac{u_i^{peak}}{u_o^{peak}}$,

where u_i^{peak} is peak displacement of incident wave, u_o^{peak} is peak displacement of

surface receiver. We define relative error $R = \frac{|\tau - \tau_0|}{\tau_0}$, where $\tau_0 = \frac{1}{2}$ is theoretical value.

The relative error $R = 0.01556$ in the validation experiment shows that our algorithm is feasible.

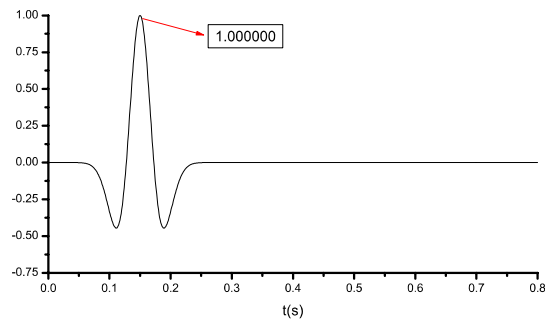


Fig.1 Displacement time travel curve of incident wave in homogeneous medium.

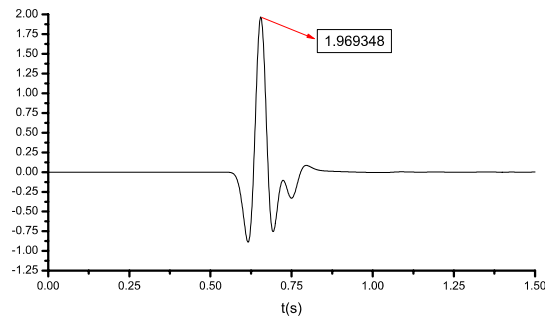


Fig.2 Displacement time travel curve of surface receiver in homogeneous medium.

Due to our simulation with P-SV plane wave, we need consider whether Rayleigh surface wave exists in numerical simulation. Rayleigh wave is formed by the interference of P wave and S wave at the free surface. Rayleigh wave exists in homogeneous medium without dispersion. We use the peak value of vertical displacement component and horizontal displacement component to draw the curves with depth. The curves show typical elliptical polarization phenomenon in Fig.3. In addition, the energy rapidly attenuates with depth increasing. We validate that Rayleigh surface wave exists during the simulation by P-SV plane wave incidence.

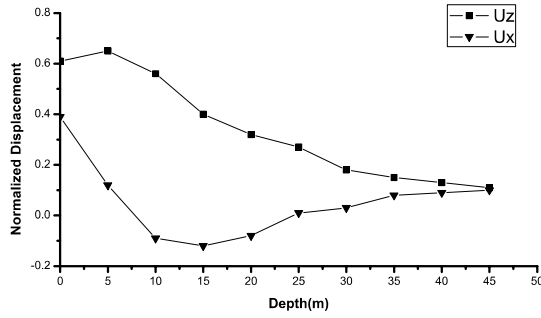


Fig.3 Curve of peak values on vertical displacement and lateral displacement with depth in homogeneous medium.

Numerical Experiments

We consider 2-D simplified sedimentary basin models to estimate the amplification effect compared with elastic layered half-space model. The simplified sedimentary basin models are built as trapezoid basin model. Building the trapezoid basin model is to show the corner effect with different inclination θ . We define the width-to-depth ratio $\alpha = \frac{w}{h}$, and compare the basin models with different inclination θ but the same ratio α . The width w is limited to the upper surface's width in basin model. The depth h is the depth of the basin model. The $b = w - 2h \cot \theta$ is the width of the basin bottom. We also define the dimensionless frequency $\eta = \frac{h}{\lambda}$, that is, the ratio of the basin depth h to the incident wavelength λ , $\lambda = \frac{c}{f_p}$, c is wave velocity, f_p is peak frequency of incident wave.

When we increase the basin depth h to reach a certain value η , we find that the amplitude of surface wave is larger than body wave's amplitude. It is effected by the basin structure. The computation model is showed in Fig.4.

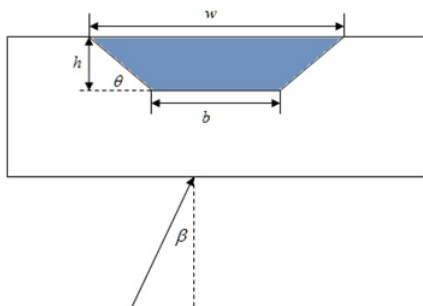


Fig.4 The computation model.

We simulate two groups of experiment including depth effect and wave velocity effect. In depth effect experiment, we compare the basin models with different basin depth but the same inclination θ . In wave velocity effect experiment, we compare the basin models with different basin wave velocity but the same bed rock.

We show the body wave peak values of displacement, velocity and acceleration on earth's surface from different depth of basin models in Fig.5. Also we show the surface wave peak values in Fig.6. The computation models are the same inclination of basin.

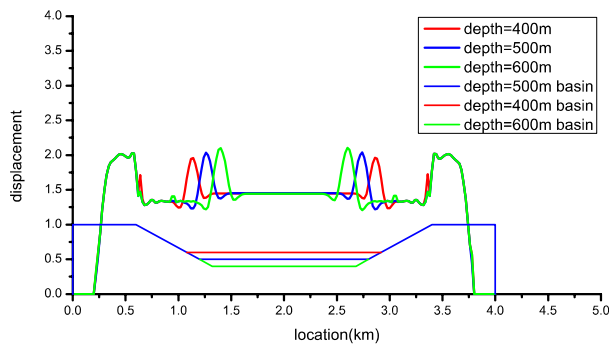


Fig.5(a) Body wave peak values of displacement on earth's surface from different depth of basin models.

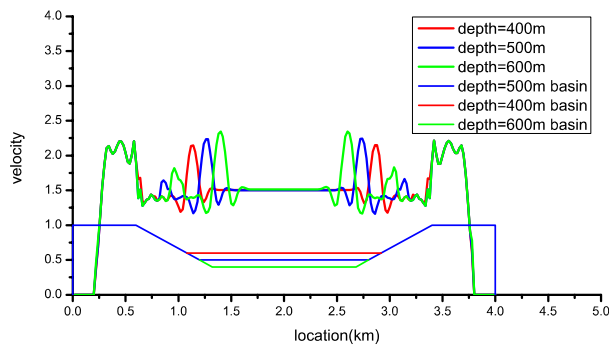


Fig.5(b) Body wave peak values of velocity on earth's surface from different depth of basin models.

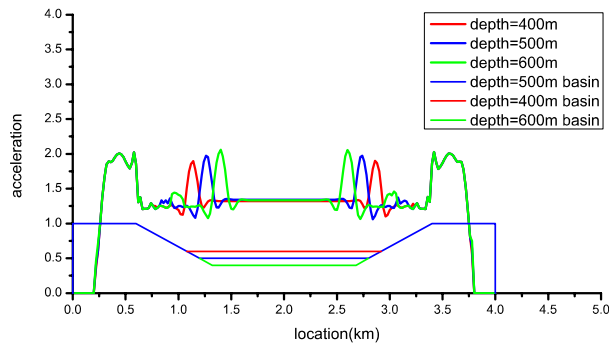


Fig.5(c) Body wave peak values of acceleration on earth's surface from different depth of basin models.

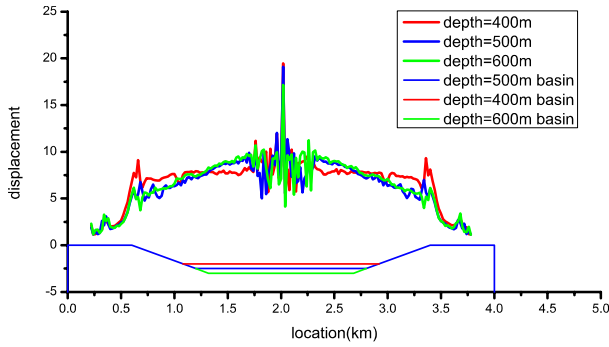


Fig.6(a) surface wave peak values of displacement on earth's surface from different depth of basin models.

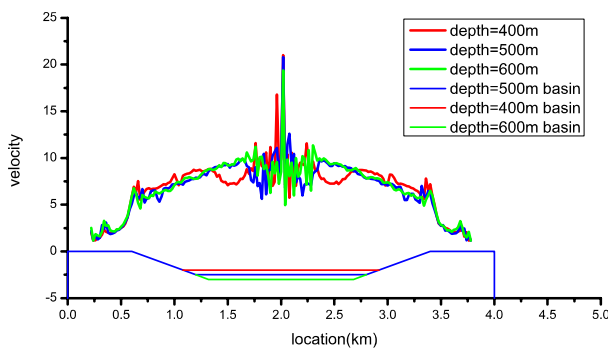


Fig.6(b) surface wave peak values of velocity on earth's surface from different depth of basin models.

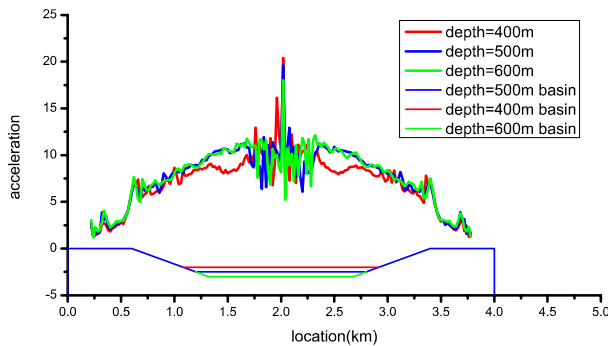


Fig.6(c) surface wave peak values of acceleration on earth's surface from different depth of basin models.

We show the body wave peak values of displacement, velocity and acceleration on earth's surface from different wave velocity of basin models in Fig.7. Also we show the surface wave peak values in Fig.8. The computation models are the same bed rock with 1000m/s S wave velocity.

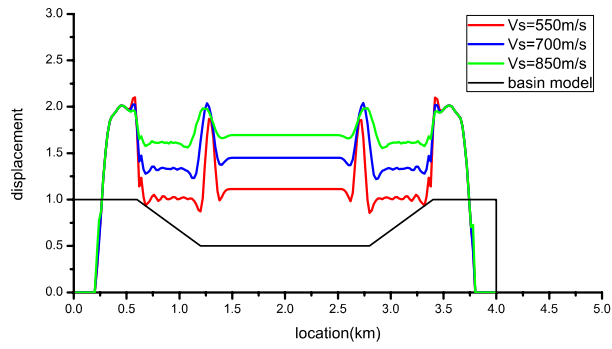


Fig.7(a) Body wave peak values of displacement on earth's surface from different wave velocity of basin models.

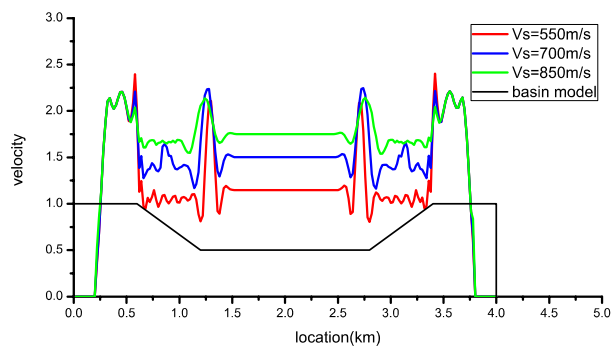


Fig.7(b) Body wave peak values of velocity on earth's surface from different wave velocity of basin models.

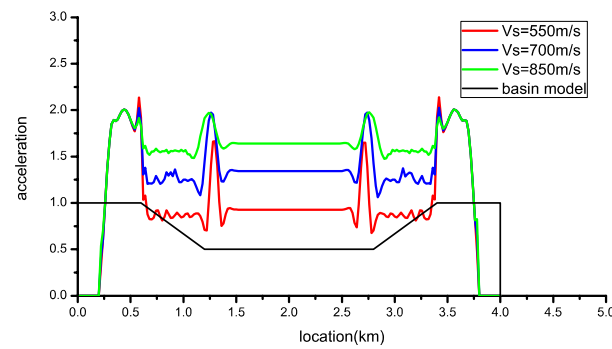


Fig.7(c) Body wave peak values of acceleration on earth's surface from different wave velocity of basin models.

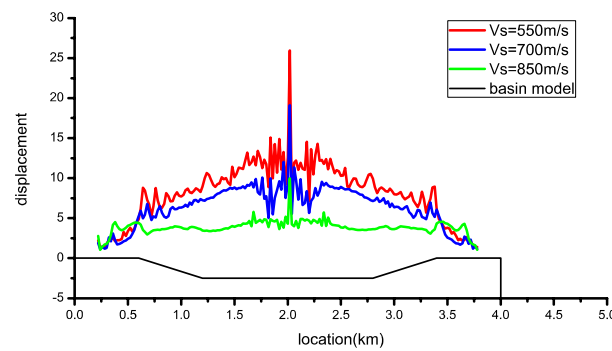


Fig.8(a) Surface wave peak values of displacement on earth's surface from different wave velocity of basin models.

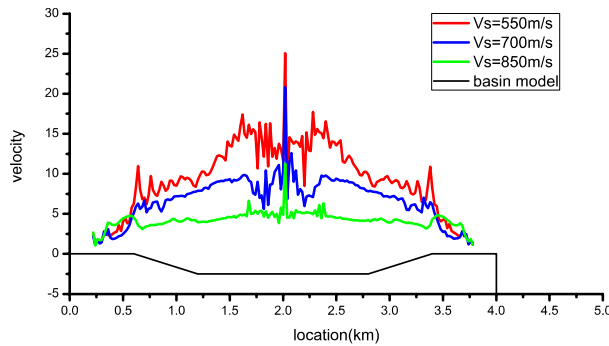


Fig.8(b) Surface wave peak values of velocity on earth's surface from different wave velocity of basin models.

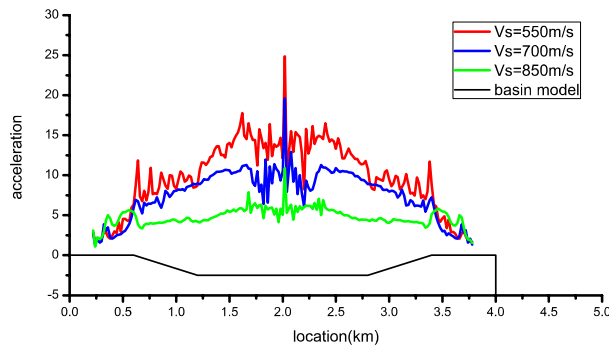


Fig.8(c) Surface wave peak values of acceleration on earth's surface from different wave velocity of basin models.

Discussion

Basin depth effect experiments tell us that the more depth of basin gets, the bigger body wave peak value at the corner area of basin on earth's surface becomes. And the body wave peak value at the center region on earth's surface does not change with variant basin depth. In addition, the more depth of basin gets, the bigger surface wave peak value at the center region on earth's surface becomes.

Basin wave velocity effect experiments tell us the difference of wave velocity between basin and bed rock is greater, then the body wave peak value is smaller. And the body wave peak value at the corner area intensely changes. In addition, the difference of wave

velocity between basin and bed rock is greater, then the surface wave peak value is bigger, especially at the center basin area.

Acknowledgement

This work has been supported by the National Natural Science Foundation of China (Grant No.41204046, 42574051).

Reference

Berenger, J. P. (1994). A perfectly matched layer for absorption of electromagnetic waves, *J. Comput. Physics*. 114, 185-200.

Chen, J. B. (2009). Lax-Wendroff and Nyström methods for seismic modeling, *Geophys. Prospect*. 57, 931-941.

Dablain, M. A. (1986). The application of high-order differencing to the scalar wave equation, *Geophysics*. 51, 54-66.

Dormy, E., and A. Tarantola (1995). Numerical simulation of elastic wave propagation using a finite volume method, *J. Geophys. Res.* 100, 2123-2133.

Feng, B. F., and G. W. Wei (2002). A comparison of the spectral and the discrete singular convolution schemes for the KdV-type equations, *J. Comput. Appl. Math.* 145, 183-188.

Frankel, A., and J. Vidale (1992). A three-dimensional simulation of seismic waves in the Santa Clara Valley, California, from a Loma Prieta aftershock, *Bull. Seism. Soc. Am.* 82, 2045-2074.

Frankel, A., and W. Stephenson (2000). Three-dimensional simulations of ground motions in the Seattle region for earthquakes in the Seattle fault zone, *Bull. Seism. Soc. Am.* 90, 1251-1262.

Iwatsu, R. (2009). Two new solutions to the third-order symplectic integration method, *Phys. Lett. A*. 373, 3056-3060.

Komatitsch, D., and J. Tromp (2002). Spectral-element simulation of global seismic wave propagation-I. Validation, *Geophys. J. Int.* 149, 390-412.

Kosloff D D, Baysal E. (1982). Forward Modeling by a Fourier Method. *Geophysics*, 47(10):1402-1412.

Li, X. F., Y. Q. Li, M.G. Zhang, and T. Zhu (2011). Scalar Seismic-Wave Equation Modeling by a

Multisymplectic Discrete Singular Convolution Differentiator Method, *Bull. Seism. Soc. Am.* 101, 1710-1718.

Li, Y. Q., X. F. Li, and M. G. Zhang (2012). Elastic Wavefield Modeling by the Symplectic Discrete Singular Convolution Differentiator Method, *Chinese J. Geophys.* 55, no.3, 343-351.

Ma, X., D. H. Yang, and J. H. Zhang.(2010). Symplectic Partitioned Runge-Kutta method for solving the acoustic wave equation, *Chinese J. Geophys.* (in Chinese), 53, no.8, 1993-2003.

Mora, P. (1986). Elastic finite-difference with convolutional operators, *Stanford Explor. Proj.* 48, 272-289.

Olsen, K. B., and G. T. Schuster (1995). Causes of low-frequency ground motion amplification in the Salt Lake Basin: the case of the vertically incident P wave, *Geophys. J. Int.* 122, 1045-1061.

Olsen, K. B., and R. J. Archuleta (1996). Three-dimensional simulation of earthquakes on the Los Angeles Fault System, *Bull. Seism. Soc. Am.* 86, 575-596.

Qin, M. Z., and W. J. Zhu (1991). Canonical Runge-Kutta-Nyström methods for second order ODE's, *Comput. Math. Appl.* 22, 85-95.

Qin, Z. (2009). Improvement of PML Absorbing Boundary Conditions in Elastic Wave Forward Modeling, *Earth Science- J. China University of Geosciences.* 34, 658-664. (in chinese).

Takeuchi, N., and R. J. Geller (2000). Optimally accurate second-order time-domain finite difference scheme for computing synthetic seismograms in 2-D and 3-D media, *Phys. Earth Planet. In.* 119, 99-131.

Virieux, J. (1984). SH-wave propagation in heterogeneous media: velocity-stress finite-difference method. *Geophysics.* 49, 1933-1957.

Yomogida, K., and J. T. Etgen (1993). 3-D wave propagation in the Los Angeles basin for the Whittier-Narrows earthquake, *Bull. Seism. Soc. Am.* 83, 1325-1344.